

MIT Open Access Articles

*Thermal conductivity of silicon nanowire
arrays with controlled roughness*

The MIT Faculty has made this article openly available. **Please share** how this access benefits you. Your story matters.

Citation: Feser, Joseph P., Jyothi S. Sadhu, Bruno P. Azeredo, et al. Thermal Conductivity of Silicon Nanowire Arrays with Controlled Roughness. *Journal of Applied Physics* 112(11): 114306, 2012. © 2012 American Institute of Physics

As Published: <http://dx.doi.org/10.1063/1.4767456>

Publisher: American Institute of Physics (AIP)

Persistent URL: <http://hdl.handle.net/1721.1/78624>

Version: Final published version: final published article, as it appeared in a journal, conference proceedings, or other formally published context

Terms of Use: Article is made available in accordance with the publisher's policy and may be subject to US copyright law. Please refer to the publisher's site for terms of use.



Thermal conductivity of silicon nanowire arrays with controlled roughness

Joseph P. Feser, Jyothi S. Sadhu, Bruno P. Azeredo, Keng H. Hsu, Jun Ma et al.

Citation: *J. Appl. Phys.* **112**, 114306 (2012); doi: 10.1063/1.4767456

View online: <http://dx.doi.org/10.1063/1.4767456>

View Table of Contents: <http://jap.aip.org/resource/1/JAPIAU/v112/i11>

Published by the [American Institute of Physics](#).

Additional information on *J. Appl. Phys.*

Journal Homepage: <http://jap.aip.org/>

Journal Information: http://jap.aip.org/about/about_the_journal

Top downloads: http://jap.aip.org/features/most_downloaded

Information for Authors: <http://jap.aip.org/authors>

ADVERTISEMENT



AIP Advances

Now Indexed in
Thomson Reuters
Databases

Explore AIP's open access journal:

- Rapid publication
- Article-level metrics
- Post-publication rating and commenting

Thermal conductivity of silicon nanowire arrays with controlled roughness

Joseph P. Feser,^{1,2,a)} Jyothi S. Sadhu,³ Bruno P. Azeredo,³ Keng H. Hsu,³ Jun Ma,³ Junhwan Kim,³ Myunghoon Seong,³ Nicholas X. Fang,⁴ Xiuling Li,⁵ Placid M. Ferreira,³ Sanjiv Sinha,³ and David G. Cahill^{1,2}

¹Department of Materials Science and Engineering, University of Illinois, Urbana, Illinois 61801, USA

²Materials Research Laboratory, University of Illinois, Urbana, Illinois 61801, USA

³Department of Mechanical Engineering, University of Illinois, Urbana, Illinois 61801, USA

⁴Department of Mechanical Engineering, Massachusetts Institute of Technology, Boston, Massachusetts, 02139, USA

⁵Department of Electrical and Computer Engineering, University of Illinois, Urbana, Illinois 61801, USA

(Received 14 September 2012; accepted 29 October 2012; published online 3 December 2012)

A two-step metal assisted chemical etching technique is used to systematically vary the sidewall roughness of Si nanowires in vertically aligned arrays. The thermal conductivities of nanowire arrays are studied using time domain thermoreflectance and compared to their high-resolution transmission electron microscopy determined roughness. The thermal conductivity of nanowires with small roughness is close to a theoretical prediction based on an upper limit of the mean-free-paths of phonons given by the nanowire diameter. The thermal conductivity of nanowires with large roughness is found to be significantly below this prediction. Raman spectroscopy reveals that nanowires with large roughness also display significant broadening of the one-phonon peak; the broadening correlates well with the reduction in thermal conductivity. The origin of this broadening is not yet understood, as it is inconsistent with phonon confinement models, but could derive from microstructural changes that affect both the optical phonons observed in Raman scattering and the acoustic phonons that are important for heat conduction. © 2012 American Institute of Physics. [<http://dx.doi.org/10.1063/1.4767456>]

I. MOTIVATION

Silicon has historically been considered an inefficient material for thermoelectric energy conversion due to its exceptionally high thermal conductivity. However, most of the heat in Si is carried by phonons with mean-free-path (MFP) larger than 300 nm.^{1,2} For comparison, the MFP of electronic carriers is ≈ 10 nm for a *n*-type carrier density of 10^{19} cm⁻³.³ Thus, the thermal conductivity of Si may be reduced without reducing the mobility of charge carriers by utilizing boundaries separated on nanometer length-scales. Nanowires,⁴ thin films,^{5,6} nanomeshes,^{7,8} and polycrystals⁹ have each been shown to be effective methods of reducing thermal conductivity when characteristic dimensions fall into the nanoscale regime.

Competitive thermoelectric materials must possess a figure-of-merit, $ZT = S^2\sigma T/\kappa$, on the order of unity; here S is the Seebeck coefficient, σ is the electrical conductivity, T is the absolute temperature, and κ is the thermal conductivity. For Si at room temperature, this requires that the lattice thermal conductivity be ≈ 1 W/m-K. Even ignoring the negative effects of boundaries on electronic properties, the Casimir calculation^{10,11} for boundary-scattering dominated heat conduction indicates that small feature sizes (~ 2 nm) should be required to make Si a viable thermoelectric; the room temperature thermal conductivity of amorphous Si itself is 1.6–4 W/m-K depending on the method of preparation.^{12,13}

Hochbaum *et al.*¹⁴ have reported measurements of suspended individual nanowires that show additional reductions are achieved by roughening the surface of the nanowires, with a 52 nm diameter wire achieving a low thermal conductivity of 1.6 W/m-K; this result is surprising since classical theories, which assume fully diffuse scattering at the boundary, predict a much higher thermal conductivity. The origin of the reduction is not currently understood, and the ultimate limits of the roughening approach are not clear. Recently, Hippalgaonkar *et al.*¹⁵ used electron beam lithography (EBL) to define roughness on the outer edge of a suspended wire and found the thermal conductivity was reduced more modestly ($\sim 30\%$ below the Casimir limit), which they attributed to the different correlation lengths of roughness between EBL-grown nanowires (where the correlation length is > 130 nm) and nanowires prepared by electroless etching (EE) (correlation length¹⁵ ~ 60 nm) such as those of the original report.¹⁴ Another recent study has compared thermal conductivity of individual Si nanowires with their corresponding high-resolution transmission electron microscopy (HRTEM)-determined edge profiles.¹⁶ That study concluded that the roughness power spectrum fits well to a power law behavior, and that the prefactor of the power law correlates to the thermal conductivity.

Theoretical approaches to understand this initial report are in disagreement over whether reduction below the Casimir limit can happen and also over the physics responsible.^{17–20} While two theoretical studies^{17,18} claim good agreement with the published data, they disagree on the mechanism. Molecular dynamics simulations^{19,20} are limited

^{a)}Author to whom correspondence should be addressed. Electronic mail: jpgfeser@uiuc.edu.

to wire diameters much smaller than the measured ones. The authors of Ref. 20 conclude that a reduction of thermal conductivity significantly below the Casimir limit requires roughness greater than 20% of the wire diameter even in wires 4 nm in diameter. While the picture remains inconclusive, the unifying theme in a majority of the theoretical effort is consideration of wave-like phonon transport, otherwise neglected in traditional particle relaxation-time approaches.

In the current paper, we use time domain thermoreflectance (TDTR) to experimentally study the thermal properties of arrays of vertically aligned Si nanowire with controlled roughness. TDTR has several advantages over the conventional approach of measuring a single nanowire using microfabricated test platforms: (1) Since the nanowires remain integrated to the substrate, the potential for nanowire damage by the scraping process is minimized; (2) A large number of nanowires are sampled during each experiment, typically $\sim 10^4$; (3) No microfabrication or micromanipulation is required, greatly expediting the measurement process; (4) The formation of good thermal contacts is greatly simplified, and the thermal interface conductance is easily measured.

II. FABRICATION OF NANOWIRES WITH CONTROLLED ROUGHNESS

A. Synthesis

To enhance control of the nanowire formation and roughening process, a two-step approach is used to decouple the process of making nanowires from the process of generating roughness; this is in contrast to previously reported electroless etching of Ag in which the roughening process occurs simultaneously with nanowire formation and is dependent on wafer doping concentration, with higher doping concentration leading to increased roughness; metal assisted chemical etch processes are known to generate porous structures at high doping concentrations,²¹ and it is thus advantageous to avoid the use of heavily doped wafers. The two-step approach consists of: (1) generation of smooth vertically aligned nanowires using a predefined etch pattern, and (2) the generation of roughness using a secondary metal-assisted chemical etch of nanoparticles coated onto the sidewalls of the array. This enables the study of nanowires of similar diameter, with varying degrees of roughness. We should point out that the recent report by Lim *et al.*¹⁶ used a qualitatively similar synthesis: nanowire were synthesized by the vapor-

liquid-solid (VLS) method, and then roughened by a secondary Ag metal-assisted chemical etch.

In the current work, the process begins with a lightly doped n-type Si wafer, $\sim 10 \Omega \text{ cm}$ (phosphorous), $\langle 100 \rangle$ oriented with a layer of native oxide; note that because of the low doping level, electronic contribution to the thermal conductivity is negligibly small ($< 1 \times 10^{-4} \text{ W/m-K}$). A thin layer of Ag ($\sim 10 \text{ nm}$ as measured by a calibrated quartz crystal monitor) is then deposited by e-beam evaporation and subsequently annealed at 350°C for 4 h under $3\text{--}8 \times 10^{-7}$ Torr pressure which thermally dewets the Ag, forming truncated spherical particles (contact angle $> 90^\circ$) on the surface. The size of the particles and the inter-particle spacing depend on the thickness²² of the Ag as well as the annealing temperature and time; the conditions described above generated particles with average diameter $\sim 100\text{--}150 \text{ nm}$. The particles are used as a shadow mask to form a gold mesh (10 nm Au deposited by e-beam evaporation). The removal of Ag particles and lift-off of excess Au is achieved by sonicating the samples in a selective etchant ($\text{NH}_4\text{OH}(32\%):\text{H}_2\text{O}_2(30%):\text{methanol} = 1:1:2$; v:v:v). The remaining Au mesh is used as catalyst for a highly anisotropic metal-assisted chemical etch^{23–25} (MacEtch), composed of $\text{HF}(49%):\text{H}_2\text{O}_2(30%):\text{ethanol} = 13:2:19$ (v:v:v). Nanowire arrays were etched to be between 500 nm and 1200 nm in length (~ 2 min etch). Under these conditions, tapering, which depends on the HF: H_2O_2 ratio and ethanol concentration, is minimized and typical rms variation of the nanowire length is only $\sim 2\text{--}4\%$ of the total length. The Au mesh was subsequently removed using a 90 s aqua regia etch. Due to the orientation of the starting wafer, the vertically-aligned nanowires have $\langle 100 \rangle$ orientation. HRTEM images show that the wires are single crystals along their entire length, and there is no discernible porosity (Fig. 1(a), details of the HRTEM are discussed subsequently).

The as-synthesized vertical nanowire arrays were smooth with roughness between 0 and 1 nm rms, and the area fraction of all arrays was between 17% and 29% for all samples (as determined by top-view SEM on each sample). To independently introduce roughness, a nominal 6–8 nm layer of Au was deposited by sputtering using a rotating and tilting ($0\text{--}30^\circ$ with random movement) sample holder to form nanoscale islands on the sidewalls of the nanowires. A dilute MacEtch solution composed of $\text{HF}(49%):\text{H}_2\text{O}_2(30%):\text{H}_2\text{O} = 1:1:24$ (v:v:v) was then used to controllably generate roughness with the etch time determining the final degree of roughness (Fig. 1). The roughened samples ($\approx 4 \text{ cm}^2$ each) were split in

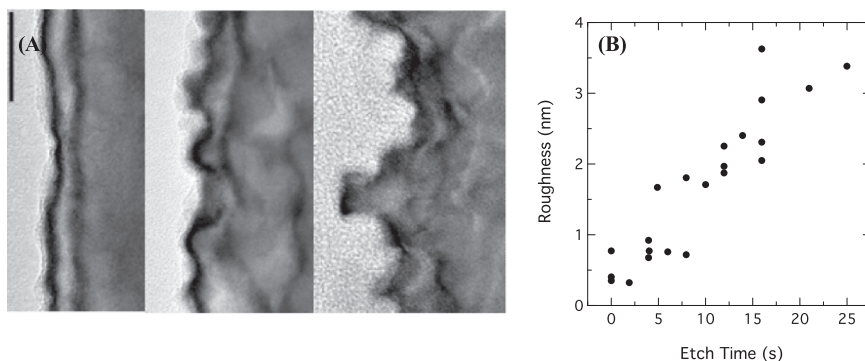


FIG. 1. (a) Bright field transmission electron micrographs of nanowires obtained by post-roughening process (etch times increasing from left to right: 2, 10, and 16 s, respectively); the scale bar in the upper left corner of the left panel is 10 nm. Nanowires are aligned along the $[110]$ zone axis. (b) rms roughness of Si nanowires after the post-roughening process, as determined from HRTEM images. Each point represents the average rms roughness for 3 wires from the same nanowire array.

two, with one sample being used for HRTEM roughness characterization and the other for TDTR measurements. HRTEM profiles do not show any discernable gradient in the roughness profiles along the length of the wires for the length of nanowires used in this study.

To create a smooth surface suitable for TDTR measurements, a commercially available spin-on glass (SOG), (Filmtronics, Siloxane 500F) was spin coated into the nanowire arrays such that the SOG was slightly thicker than the nanowires and annealed at 350 °C. The SOG was then reactively ion etched in CHF₃ until the thickness of the SOG is within ~20 nm of the nanowire as verified in side view SEM for each sample. Samples were then coated in ~70 nm Al by magnetron sputtering (with precise thickness (± 4 nm) determined by picosecond acoustics for individual samples). The reflectivity of each sample was compared to a reference sample of a smooth, oxidized Si wafer coated by Al, and all reported samples display specularly greater than 90%, with most being indistinguishable from the smooth Al reference sample to within experimental uncertainty.

B. Structural characterization

The areal fraction and size distribution of each nanowire array were measured prior to the infusion of spin-on glass by top view SEM and analyzed using the software package IMAGEJ. To prepare images for analysis, the images were thresholded and nanowires that were visibly clumped were separately manually with a 1 pixel line, so that the size distribution statistics were more representative. The apparent SEM average diameter is measured as $D_{SEM} = 1/N \sum_i^N \sqrt{4A_{SEM,i}/\pi}$, where $A_{SEM,i}$ is the area of each wire. SEM over-predicts the nanowire diameter/area when the nanowires are rough, therefore once the roughness is measured, the diameter of the nanowires is adjusted by an amount $\delta D = 2\sqrt{2}\delta_{rms}$, corresponding to twice the amplitude of an equivalent sine wave. Therefore, the diameter reported is $D = D_{SEM} - \delta D$; for the same reason, the area fraction is reduced by a factor of $(D_{SEM} - \delta D)^2/D_{SEM}^2$. For the roughest nanowires reported, this correction reduces the area fraction by ~17% and the diameter by ~9%.

Roughness of the nanowires was determined by HRTEM. A double-tilt holder was used to tilt the nanowire to [110] zone-axis enabling high resolution imaging of the Si/native-oxide boundary (<1 nm resolution). Several atomic resolution images recorded along the length of a nanowire are stitched together to generate a continuous roughness profile of the nanowire over a length of ~500 nm, with the boundary being taken as the outmost edge of the lattice fringes; the boundary profile was fit to a linear function, considered to be the mean surface and the rms roughness and correlation length were calculated with reference to the mean surface. This procedure was conducted for three nanowires from each array and on every sample.

From the HRTEM profiles, we have characterized the surface features of nanowires using the height-difference correlation function, and this has been compared to the measured thermal conductivity. The height difference correlation function (HDCF) is defined as

$$G(\rho) \equiv 1/L \int_0^L [h(x+\rho) - h(x)]^2 dx,$$

where $h(x)$ is the surface height profile and L is the length of the wire over which the integrand is computable (note that the coordinate $x + \rho$ does not always lie in the domain of the wire). The HDCF is a real space statistical measurement that gives detailed information about the length scales of the system;²⁶ in the current context, we use the HDCF to characterize the rms amplitude of roughness (σ) and determine its correlation length (ξ). The key features of the HDCF are that, typically, for $\rho < \xi$, $[G(\rho)]^{1/2} \propto \rho^h$ and approaches a constant $[G(\rho)]^{1/2} = \sqrt{2}\sigma$ when $\rho > \xi$. (For a morphology dominated by a single length scale, $h \approx 1$.) The correlation length can be estimated by the intersection of fits to these two regimes, where $\rho_c = \xi/4$. The correlation lengths for all nanowires are in a range from 15 to 40 nm which is characteristic of the size of the Au islands used during the roughening process (Fig. 3).

III. THERMAL CONDUCTIVITY MEASUREMENTS OF SILICON NANOWIRE ARRAYS USING TDTR

Time domain thermoreflectance was used to characterize the thermal conductivity of the roughened Si nanowire arrays. Our measurement system and methods of data reduction have been described in detail previously.^{27,28} The time evolution of surface temperature is measured through temperature-dependent changes in the reflectivity, i.e., the thermoreflectance. We analyze the ratio of in-phase, $V_{in}(t)$ and out-of-phase $V_{out}(t)$, variations in the intensity of the reflected probe beam at the modulation frequency, f , of the pump beam as a function of delay time, t , between pump and probe.²⁸ The wavelength of the mode-locked Ti:sapphire laser is $\lambda = 785$ nm and the $1/e^2$ radius of both focused beams is $14 \mu\text{m}$. Pump and probe laser power were set to 20 mW and 14 mW, respectively, which is calculated to produce <1 K steady state temperature rise. Aluminum transducer thickness was measured using picosecond acoustics. Our TDTR approach has been thoroughly validated and extensively applied in studies of the thermal conductivity of thin films²⁹ and the thermal conductance of interfaces.³⁰

However, for nanowire arrays embedded in a host matrix material there are several unique aspects to the data acquisition and reduction. Koh *et al.*³¹ have previously reported that thin film composites of vertically aligned InAs nanowire arrays with poly(methyl methacrylate) matrix filler display effective properties that depend on the modulation frequency, and an effective thermal interface conductance well-below any known physical interface. We observe this to be true for the current Si nanowire arrays as well (Fig. 2). Low effective thermal interface conductance is due to the fact that most of the heat is channeled through the nanowire which, due to the low area fraction, amplifies its effective interface resistance by an amount, $\sim 1/x$, where x is the area fraction of nanowires. In the current study, effective thermal interface conductances are observed to be between 25–40 MW/m²-K, consistent with a 20–30% areal fraction of nanowires.

The frequency-dependence of the composite thermal conductivity can be understood by examining the origin of

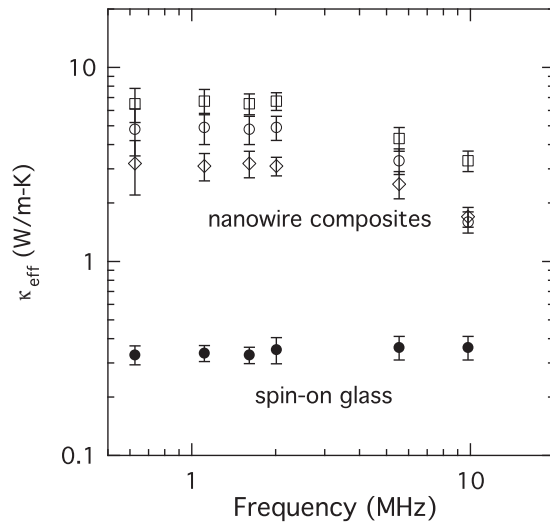


FIG. 2. Effective thermal conductivity of several nanowire composite layers (open circles) measured as a function of the modulation frequency. The spin-on-glass (solid circles) displays no significant frequency dependence. The low frequency limit of the measurements is used in conjunction with Eqs. (2) and (3) to determine the thermal conductivity of the nanowires.

the out-of-phase signal in TDTR. The out-of-phase signal depends sensitively on the surface temperature response to a sinusoidal heat input at the modulation frequency,²⁸ which arises from “pulse accumulation,”³³ (i.e., there is insufficient time between pulses for the surface temperature to decay to its initial temperature). At high modulation frequency, the diffusion distance for heat in the matrix material is much smaller than the distance between adjacent nanowires. Thus, temperature is not uniform in the lateral direction except at the surface, where the array is connected by a high thermal

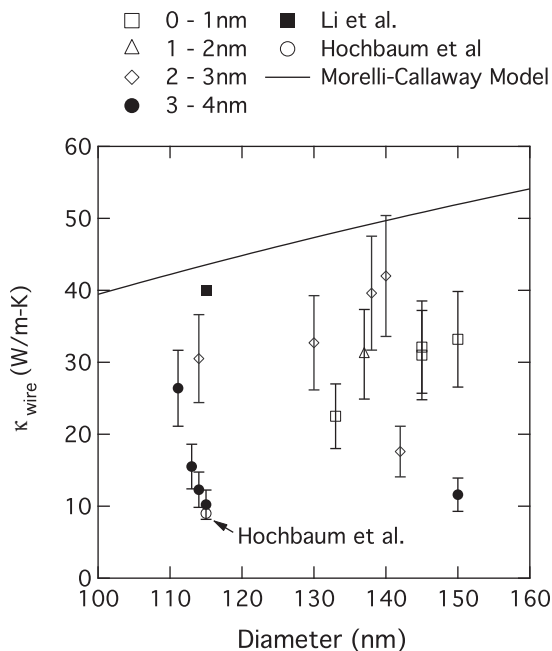


FIG. 3. Measured silicon nanowire thermal conductivity for arrays of varied rms roughness. Also shown are the theoretical prediction is based on the Morelli-Callaway model,³² and previous measurements of a single VLS-grown smooth nanowire⁴ and a single EE rough nanowire¹⁴ for comparison.

conductivity metal. In this limit, the heat flux divides such that that the average response at the surface is indistinguishable from an effective medium with effusivity,

$$\sqrt{(\kappa C)_{\text{eff}}} = x\sqrt{(\kappa C)_{\text{wire}}} + (1-x)\sqrt{(\kappa C)_{\text{SOG}}}. \quad (1)$$

Here κ and C are the thermal conductivity and volumetric heat capacity, respectively. However, at low frequency, heat fully penetrates the matrix material in the lateral direction, so that the temperature is roughly isothermal in-plane. In this case, the surface temperature response is indistinguishable from that of an effective medium with

$$C_{\text{eff}} = xC_{\text{wire}} + (1-x)C_{\text{SOG}}, \quad (2)$$

$$\kappa_{\text{eff}} = x\kappa_{\text{wire}} + (1-x)\kappa_{\text{SOG}}. \quad (3)$$

In the intermediate frequency range, the behavior cannot be captured by a simple effective medium model. Transient finite element analysis is capable of modeling the intermediate cases; however, performing the simulation of TDTR data requires a summation over the frequency response at thousands of frequencies for each time-delay curve,²⁸ which was not practical. Rather, finite element calculations were used only to verify that the transition from the high to low frequency regime is controlled by the thermal diffusion distance in the spin-on-glass compared to the nanowire spacing, and that at the lowest experimental frequencies, the frequency response is well-represented by the effective medium theory in Eqs. (2) and (3); Koh used a similar approach in his study of InAs nanowire arrays by TDTR.³¹

The measurements at either modulation frequency limit can be used as a simple way to determine the thermal conductivity of the nanowires, κ_{wire} . In the current work, the low frequency limit is used since it is sensitive to the properties deeper within the nanowire arrays and is less sensitive to knowledge of the matrix properties. This requires that the properties of the filler SOG be known; the properties of a pure SOG film (220 nm) were measured at two modulation frequencies (1.6 MHz and 9.8 MHz) to separately determine the thermal conductivity (0.36 ± 0.3 W/m-K) and specific heat capacity (1.3 ± 0.1 MJ/m³-K); the thermal conductivity is close to previously measured spin-on-glass with similar composition (~ 0.38 W/m-K),^{34,35} and the specific heat capacity is near that of other siloxanes such as PDMS (1.3–1.5 MJ/m³-K).³⁶

From the low frequency limit of the composite thermal conductivity, the thermal conductivity of the nanowires is then extracted using Eqs. (2) and (3). The extracted values are plotted in Fig. 3. The error-bars for the measurement are larger than typical for TDTR measurements ($\sim 20\%$ instead of $\sim 10\%$)²⁹ for several reasons; in addition to the usual error contributions coming from uncertainty in the transducer thickness and heat capacity ($\sim 8\%$ together),²⁹ there is uncertainty in the nanowire length ($\sim 10\%$), the areal fraction of nanowires ($\sim 10\%$ uncertainty based on SEM images at various locations on the chips), and a significant error in the phase of the reference channel due to the lower signal-to-noise ratio and smaller jump in the in-phase signal at zero time delay that occurs at low frequency²⁹ (up to 10% in some cases).

Time-domain thermoreflectance measurements show that nanowire arrays with low roughness have the highest thermal conductivity, albeit slightly below what has been observed in the case of a similarly sized nanowire grown by a VLS process.⁴ Previously measured VLS nanowires all have been [111] oriented, whereas in the current study [100] oriented wire were produced, due to the orientation of the starting wafer. In the Casimir regime, the thermal conductivity of [111] oriented wires are expected to be $\sim 50\%$ smaller than [100] wires, due to phonon focusing effects;¹⁰ however, comparing the current data to the single nanowire measurement of Li *et al.*,⁴ that behavior was not observed. In qualitative agreement Hochbaum *et al.*,¹⁴ several highly roughened nanowire arrays are observed with thermal conductivity well below what is explainable from boundary scattering from the nanowire sidewalls (Figure 3), with our lowest measured values near 10 W/m-K.

In Fig. 3, we have adopted the model developed by Morcelli³² to predict the expected thermal conductivity. The basic elements of the model are that: (1) it is a modified version of the Callaway model;³⁷ (2) phonon dispersion is treated as isotropic and linear with an energy cutoff determined by the maximum energy of the acoustic branch rather than a Debye frequency; (3) three distinct polarizations are treated; (4) mode-dependent scattering rates are calculated using Matthiessen's rule, considering normal and Umklapp phonon-phonon processes, isotope scattering, and boundary scattering where the boundary scattering length is taken as the diameter of the nanowire in our case. The model implicitly neglects anisotropic effects such as phonon focusing and conduction by optical phonons, but correctly predicts the thermal conductivity of individual Si nanowires measured by Li *et al.*⁴ Comparing our experimental results to the predicted values for nanowires in this size range, the lowest thermal conductivities measured are about 4 times lower than would be expected based on fully diffuse boundary scattering.

Based on the limited range of correlation lengths produced, we cannot determine if there is any dependence of the thermal conductivity on correlation length (Fig. 4(b)). The thermal conductivity of our samples do correlate with rms roughness, σ (Fig. 4(c)). However, it is difficult to distin-

guish whether the roughness is the origin of the reduced thermal conduction, or rather if there are other microstructural changes that are associated with the etching process.

IV. PROBING MICROSTRUCTURE USING RAMAN SPECTROSCOPY

Raman scattering was employed to gain more insight into the microstructure of the arrays. Numerous studies document Raman scattering from bulk Si,³⁸ amorphous Si,³⁹ and various nanostructured intermediates such as nanocrystals,^{40–42} porous Si,⁴³ and nanowires.^{44,45} For bulk Si in the backscattering geometry, the primary feature of the Raman signal is a sharp peak occurring near 520 cm^{-1} generated by the zone-center LO phonon, with intrinsic full-width at half-maximum (FWHM)³⁸ $\sim 2.6\text{ cm}^{-1}$ corresponding to an energy relaxation timescale of $\sim 2.1\text{ ps}$.⁴⁶ In nanostructures, the momentum selection rules for scattering are relaxed such that phonons with wavevector $q \sim 1/L$ also contribute,⁴² where L is the characteristic size of the structure. This relaxation of selection rules has the effect of broadening the energy spectrum of Raman-active phonons and slightly lowering the average energy of the first-order scattering peak. However, in nanowires with diameter $>100\text{ nm}$ the effect of phonon confinement is expected to be small, with less than 0.02% change in broadening in the linewidth and less than 0.01 cm^{-1} red-shift in the peak location.⁴⁵

The Stokes shift in the backscattering geometry was collected using a 488 nm laser focused to a $5\text{ }\mu\text{m}$ $1/e^2$ radius with 2 mW intensity. The signal was analyzed using an Acton InSight spectrometer with $2.0\text{ cm}^{-1}/\text{pixel}$ bandwidth. We estimate that the laser power of 2 mW produces less than a 10 K steady state temperature rise in the lowest thermal conductivity samples; we verified that the Raman peakwidths and peak positions do not depend on laser intensity. The measured peakwidth of bulk Si in our system is 4.24 cm^{-1} ; treating the measured intensity as a Lorentzian convolved with Gaussian function that describes the instrumental broadening,³⁸ and using the bulk Si peakwidth of 2.6 cm^{-1} ,³⁸ the FWHM of the instrumental broadening is $\sim 2.6\text{ cm}^{-1}$.

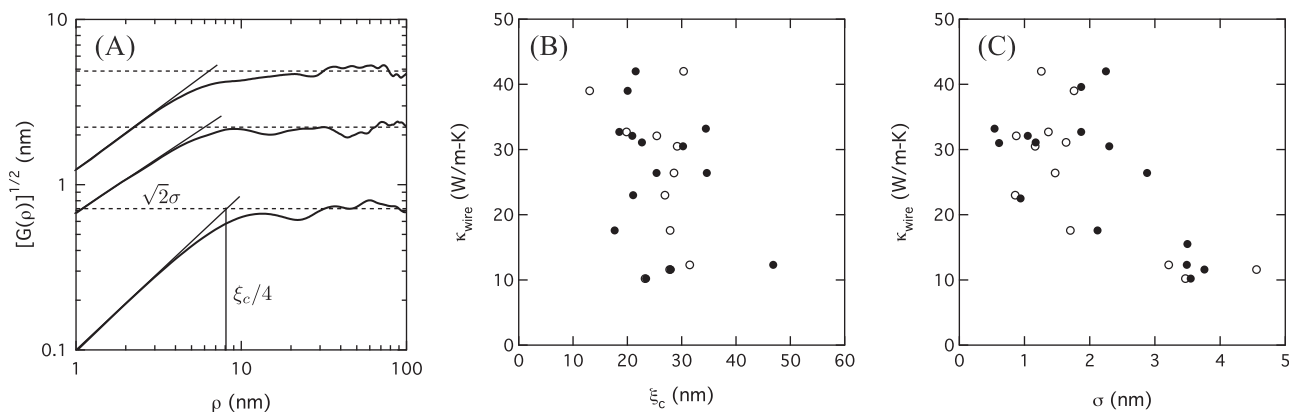


FIG. 4. (a) Height difference correlation functions measured for three representative nanowire arrays. (b) Thermal conductivity versus correlation length, ξ_c ; solid and open circles are for nanowire profiles taken as the Si-SiO₂ interface and air-SiO₂ interface respectively. (c) Thermal conductivity versus rms roughness, σ .

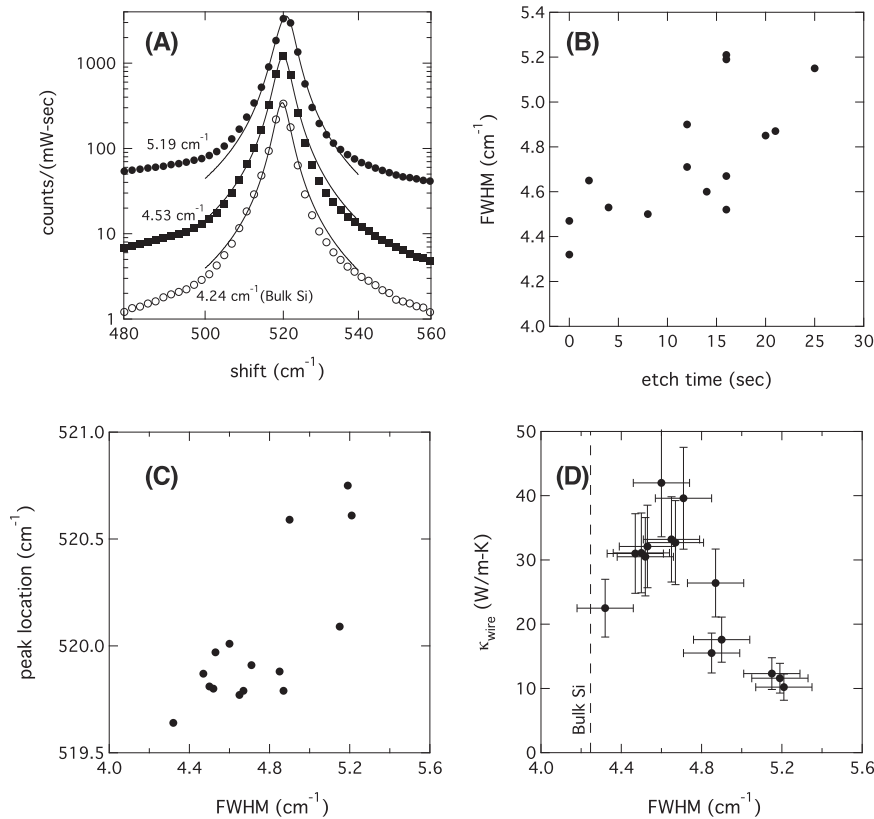


FIG. 5. (a) Raman scattering intensity for a 3.5 nm rms roughness nanowire array (solid circles), a 1.0 nm rms roughness nanowire array (solid square), and bulk silicon (open circles); Solid lines are best fit curves to the model, and the adjacent numbers are the associated FWHM. The open squares and its fit are scaled by 0.25 to avoid visual overlap with the solid circles. (b) Raman FWHM plotted against the etching time of the roughening process. (c) the position of the Raman peak plotted against the Raman FWHM. (d) The thermal conductivity of each nanowire array plotted against the corresponding Raman FWHM.

Despite expectations based on phonon-confinement, the Raman intensity of our nanowire arrays do show significant broadening that increases with etch time of the roughening process (Fig. 5). In addition, we see that the thermal conductivity of the nanowire arrays only have low values when their associated linewidth is broadened (Fig. 5(d)). The Raman intensity profiles are not fully consistent with phonon confinement in nanostructures, which would be expected to have red-shifted peak locations, unless a large compressive stress is also present. Based on previous measurements of silicon under uniaxial compressive stress that show a blue-shift of $\sim 0.004 \text{ cm}^{-1}/\text{MPa}$,⁴⁷ we estimate that the approximate magnitude of the associated stress would need to be $\sim 300 \text{ MPa}$. In addition, the length-scales indicated by the classical Raman phonon confinement model⁴⁵ appear to be too small to be directly related to the acoustic wave scattering from boundaries. Our modified-Callaway model requires boundary scattering lengths $\geq 30 \text{ nm}$ to explain the current thermal conductivity measurements, whereas interpreting the Raman FWHM as phonon confinement would predict boundaries spaced on $\sim 10 \text{ nm}$ scale for the roughest wires.

An alternative possibility is that the broadening originates from crystal disorder induced by the etching process. While we know of no precedent for this with respect to the metal-assisted chemical etching, in previous studies overabundance of H_2O_2 with respect to HF has been observed to generate porous Si away from the metal catalyst.²³ We do not observe discernable porosity by HRTEM, and both MacEtch solutions utilize a high ratio of HF: H_2O_2 to avoid porosity. However, it is possible that clusters of point defects, which would be difficult to detect by TEM, could form beneath the surface of the nanowire. In that case, disorder

is capable of relaxing the selection rules for Raman scattering, leading to spectrum broadening.⁴⁸

Thus, whatever the origin of the altered Raman line-shape, it is likely to be indicative of microstructural changes caused by the etching process. If the microstructure changes in such a way that acoustic phonon scattering is increased, then this provides an alternative hypothesis to explain thermal conductivity reductions that does not depend on the roughness itself. Note that research has yet to show whether thermal conductivity increases upon removing roughness, and thus this hypothesis cannot be ruled out.

V. CONCLUSION

In summary, a technique for fabricating vertically aligned Si nanowires with controlled roughness based on a two-step wet etch process has been presented and used to study the thermal transport properties of rough Si nanowires with similar diameter and surface correlation length using time-domain thermoreflectance. The measured thermal conductivity of highly roughened nanowires are found to be significantly below the boundary scattering limit predicted based on a modified Callaway model and below that previously measured for smooth single nanowires of similar diameter. The lowest thermal conductivities are similar to that previously reported on individual roughened nanowires. However, in all nanowire arrays with low thermal conductivity, we observe significantly broadened Raman linewidths. The broadening may indicate the presence of microstructural changes that affect both the optical phonons observed in Raman scattering and the acoustic phonons that are important for heat conduction. This suggests that reductions in the

thermal conductivity may not be due to the nanowire roughness, but rather to microstructural changes introduced by the metal-assisted chemical etching process.

ACKNOWLEDGMENTS

This work was supported by the Advanced Research Projects Agency–Energy (ARPA-E) under Contract No. DOE-DE-AR-0000041PF-ARRA. This work was carried out in part in the Frederick Seitz Materials Research Laboratory Central Facilities and the Micro and Nano Laboratory at the University of Illinois.

- ¹C. Dames and G. Chen, in *Thermoelectrics Handbook: Macro to Nano*, edited by D. M. Rowe (CRC, 2006).
- ²K. Esfarjani, G. Chen, and H. T. Stokes, *Phys. Rev. B* **84**(8), 085204 (2011).
- ³L. Weber and E. Gmelin, *Appl. Phys. A* **53**(2), 136 (1991).
- ⁴D. Y. Li, Y. Y. Wu, P. Kim, L. Shi, P. D. Yang, and A. Majumdar, *Appl. Phys. Lett.* **83**(14), 2934 (2003).
- ⁵Y. S. Ju and K. E. Goodson, *Appl. Phys. Lett.* **74**(20), 3005 (1999).
- ⁶W. J. Liu and M. Asheghi, *ASME Trans. J. Heat Transfer* **128**(1), 75 (2006).
- ⁷P. E. Hopkins, C. M. Reinke, M. F. Su, R. H. Olsson, E. A. Shaner, Z. C. Leseman, J. R. Serrano, L. M. Phinney, and I. El-Kady, *Nano Lett.* **11**(1), 107 (2010).
- ⁸J. Y. Tang, H. T. Wang, D. H. Lee, M. Fardy, Z. Y. Huo, T. P. Russell, and P. D. Yang, *Nano Lett.* **10**(10), 4279 (2010).
- ⁹S. K. Bux, R. G. Blair, P. K. Gogna, H. Lee, G. Chen, M. S. Dresselhaus, R. B. Kaner, and J. P. Fleurial, *Adv. Funct. Mater.* **19**(15), 2445 (2009).
- ¹⁰A. K. McCurdy, H. J. Maris, and C. Elbaum, *Phys. Rev. B* **2**(10), 4077 (1970).
- ¹¹H. B. G. Casimir, *Physica* **5**(6), 495 (1938).
- ¹²D. G. Cahill, M. Katiyar, and J. R. Abelson, *Philos Mag B* **71**(4), 677 (1995).
- ¹³H. S. Yang, D. G. Cahill, X. Liu, J. L. Feldman, R. S. Crandall, B. A. Sperling, and J. R. Abelson, *Phys. Rev. B* **81**(10), 104203 (2010).
- ¹⁴A. I. Hochbaum, R. K. Chen, R. D. Delgado, W. J. Liang, E. C. Garnett, M. Najarian, A. Majumdar, and P. D. Yang, *Nature* **451**(7175), 163 (2008).
- ¹⁵K. Hippalgaonkar, B. L. Huang, R. K. Chen, K. Sawyer, P. Ercius, and A. Majumdar, *Nano Lett.* **10**(11), 4341 (2010).
- ¹⁶J. W. Lim, K. Hippalgaonkar, S. C. Andrews, A. Majumdar, and P. D. Yang, *Nano Lett.* **12**(5), 2475 (2012).
- ¹⁷P. Martin, Z. Aksamija, E. Pop, and U. Ravaioli, *Phys. Rev. Lett.* **102**(12), 125503 (2009).
- ¹⁸J. Sadhu and S. Sinha, *Phys. Rev. B* **84**(11), 115450 (2011).
- ¹⁹D. Donadio and G. Galli, *Phys. Rev. Lett.* **102**(19), 195901 (2009).
- ²⁰J. Carrete, L. J. Gallego, L. M. Varela, and N. Mingo, *Phys. Rev. B* **84**(7), 075403 (2011).
- ²¹A. I. Hochbaum, D. Gargas, Y. J. Hwang, and P. D. Yang, *Nano Lett.* **9**(10), 3550 (2009).
- ²²T. W. H. Oates, H. Sugime, and S. Noda, *J. Phys. Chem. C* **113**(12), 4820 (2009).
- ²³Z. P. Huang, N. Geyer, P. Werner, J. de Boor, and U. Gosele, *Adv. Mater.* **23**(2), 285 (2011).
- ²⁴W. Chern, K. Hsu, I. S. Chun, B. P. de Azeredo, N. Ahmed, K. H. Kim, J. M. Zuo, N. Fang, P. Ferreira, and X. L. Li, *Nano Lett.* **10**(5), 1582 (2010).
- ²⁵X. Li, *Curr. Opin. Solid State Mater. Sci.* **16**(2), 71–81 (2012).
- ²⁶K. Vanormelingen, B. Degroote, and A. Vantomme, *J. Vac. Sci. Technol. B* **24**(2), 725 (2006).
- ²⁷K. Kang, Y. K. Koh, C. Chiritescu, X. Zheng, and D. G. Cahill, *Rev. Sci. Instrum.* **79**(11), 114901 (2008).
- ²⁸D. G. Cahill, *Rev. Sci. Instrum.* **75**(12), 5119 (2004).
- ²⁹Y. K. Koh, S. L. Singer, W. Kim, J. M. O. Zide, H. Lu, D. G. Cahill, A. Majumdar, and A. C. Gossard, *J. Appl. Phys.* **105**(5), 054303 (2009).
- ³⁰R. M. Costescu, M. A. Wall, and D. G. Cahill, *Phys. Rev. B* **67**(5), 054302 (2003).
- ³¹A. I. Persson, Y. K. Koh, D. G. Cahill, L. Samuelson, and H. Linke, *Nano Lett.* **9**(12), 4484 (2009).
- ³²D. T. Morelli, J. P. Heremans, and G. A. Slack, *Phys. Rev. B* **66**(19), 195304 (2002).
- ³³A. J. Schmidt, X. Y. Chen, and G. Chen, *Rev. Sci. Instrum.* **79**(11), 114902 (2008).
- ³⁴B. M. Curtin, E. W. Fang, and J. E. Bowers, *J. Electron. Mater.* **41**(5), 887–894 (2012).
- ³⁵R. M. Costescu, A. J. Bullen, G. Matamis, K. E. O'Hara, and D. G. Cahill, *Phys. Rev. B* **65**(9), 094205 (2002).
- ³⁶J. E. Mark, *Polymer Data Handbook* (Oxford University Press, New York, 1999), pp. xi.
- ³⁷J. Callaway, *Phys. Rev.* **113**(4), 1046 (1959).
- ³⁸J. Menendez and M. Cardona, *Phys. Rev. B* **29**(4), 2051 (1984).
- ³⁹M. H. Brodsky, M. Cardona, and J. J. Cuomo, *Phys. Rev. B* **16**(8), 3556 (1977).
- ⁴⁰I. F. Crowe, M. P. Halsall, O. Hulko, A. P. Knights, R. M. Gwilliam, M. Wojdak, and A. J. Kenyon, *J. Appl. Phys.* **109**(8), 083534 (2011).
- ⁴¹I. H. Campbell and P. M. Fauchet, *Solid State Commun.* **58**(10), 739 (1986).
- ⁴²H. Richter, Z. P. Wang, and L. Ley, *Solid State Commun.* **39**(5), 625 (1981).
- ⁴³S. R. Goodes, T. E. Jenkins, M. I. J. Beale, J. D. Benjamin, and C. Pickering, *Semicond. Sci. Technol.* **3**(5), 483 (1988).
- ⁴⁴K. W. Adu, H. R. Gutierrez, U. J. Kim, G. U. Sumanasekera, and P. C. Eklund, *Nano Lett.* **5**(3), 409 (2005).
- ⁴⁵S. Piscanec, M. Cantoro, A. C. Ferrari, J. A. Zapien, Y. Lifshitz, S. T. Lee, S. Hofmann, and J. Robertson, *Phys. Rev. B* **68**(24), 241312 (2003).
- ⁴⁶J. J. Letcher, K. Kang, D. G. Cahill, and D. D. Dlott, *Appl. Phys. Lett.* **90**(25), 252104 (2007).
- ⁴⁷E. Anastassakis, A. Pinczuk, E. Burstein, F. H. Pollak, and M. Cardona, *Solid State Commun.* **88**(11–12), 1053 (1993).
- ⁴⁸F. Widulle, T. Ruf, M. Konuma, I. Silier, M. Cardona, W. Kriegseis, and V. I. Ozogin, *Solid State Commun.* **118**(1), 1 (2001).